Received: 16 November 2023 | Revised: 12 October 2024 | Accepted: 4 November 2024

DOI: 10.1002/mp.17520

RESEARCH ARTICLE

MEDICAL PHYSICS

Dosimetric and biological impact of activity extravasation of radiopharmaceuticals in PET imaging

Ashok Tiwari[1,2] | **Matthew Andriotty**[3] | **Greeshma Agasthya**[3] | **John J. Sunderland**[4] | **Dustin R. Osborne**[5] | **Anuj J. Kapadia**[1]

[1]Advanced Computing for Health Sciences, Oak Ridge National Laboratory, Oak Ridge, Tennessee, USA

[2]Department of Radiation Oncology, Indiana University School of Medicine, Indianapolis, Indiana, USA

[3]Department of Nuclear & Radiological Engineering & Medical Physics, Georgia Institute of Technology, Atlanta, Georgia, USA

[4]Department of Radiology, University of Iowa, Iowa City, Iowa, USA

[5]Department of Radiology, University of Tennessee, Knoxville, Tennessee, USA

Correspondence
Ashok Tiwari, Department of Radiation Oncology, Indiana University School of Medicine, 535 Barnhill Drive RT041, Indianapolis, IN 46202, USA.
Email: astiwa@iu.edu

Funding information
U.S. Department of Energy, Grant/Award Number: DE-AC05-00OR22725

Abstract

Background: The increasing use of nuclear medicine and PET imaging has intensified scrutiny of radiotracer extravasation. To our knowledge, this topic is understudied but holds great potential for enhancing our understanding of extravasation in clinical PET imaging.

Purpose: This work aims to (1) quantify the absorbed doses from radiotracer extravasation in PET imaging, both locally at the site of extravasation and with the extravasation location as a source of exposure to bodily organs and (2) assess the biological ramifications within the injection site at the cellular level.

Methods: A radiation dosimetry simulation was performed using a whole-body 4D Extended Cardiac-Torso (XCAT) phantom embedded in the GATE Monte Carlo platform. A 10-mCi dose of ^{18}F-FDG was chosen to simulate a typical clinical PET scan scenario, with 10% of the activity extravasated in the antecubital fossa of the right arm of the phantom. The extravasation volume was modeled as a 5.5 mL rectangle in the hypodermal layer of skin. Absorbed dose contributions were calculated for the first two half-lives, assuming biological clearance thereafter. Dose calculations were performed as absorbed doses at the organ and skin levels. Energy deposition was simulated both at the local extravasation site and in multiple organs of interest and converted to absorbed doses based on their respective masses. Each simulation was repeated ten times to estimate Monte Carlo uncertainties. Biological impacts on cells within the extravasated volume were evaluated by randomizing cells and exposing them to a uniform radiation source of ^{18}F and ^{68}Ga. Particle types, their energies, and direction cosines were recorded in phase space files using a separate Geant4 simulation to characterize their entry into the nucleus of the cellular volume. Subsequently, the phase space files were imported into the TOPAS-nBio simulation to assess the extent of DNA damage, including double-strand breaks (DSBs) and single-strand breaks (SSBs).

Results: Organ-level dosimetric estimations are presented for ^{18}F and ^{68}Ga radionuclides in various organs of interest. With 10% extravasation, the hypodermal layer of the skin received the highest absorbed dose of 1.32 $\pm$ 0.01 Gy for ^{18}F and 0.99 $\pm$ 0.01 Gy for ^{68}Ga. The epidermal and dermal layers received absorbed doses of 0.07 $\pm$ 0.01 Gy and 0.13 $\pm$ 0.01 Gy for ^{18}F, and 0.14 $\pm$ 0.01 Gy and 0.29 $\pm$ 0.01 Gy for ^{68}Ga, respectively. In the extravasated volume, ^{18}F caused an average absorbed dose per nucleus of 0.17 $\pm$ 0.01 Gy, estimated to result in 10.58 $\pm$ 0.50 DSBs and 268.11 $\pm$ 12.43 SSBs per nucleus. For ^{68}Ga, the absorbed dose per nucleus was 0.11 $\pm$ 0.01 Gy, leading to an estimated 6.49 $\pm$ 0.34 DSBs and 161.24 $\pm$ 8.12 SSBs per nucleus. Absorbed doses in other organs were on the order of micro-gray (μGy).

Conclusion: The likelihood of epidermal erythema resulting from extravasation during PET imaging is low, as the simulated absorbed doses to the epidermis remain below the thresholds that trigger such effects. Moreover, the organ-level absorbed doses were found to be clinically insignificant across various simulated organs. The minimal DNA damage at the extravasation site suggests that long-term harm, such as radiation-induced carcinogenesis, is highly unlikely.

KEYWORDS
absorbed dose, DNA strand breaks, extravasation dosimetry, Monte Carlo, XCAT phantom

1 | INTRODUCTION

The use of nuclear medicine imaging procedures in clinical settings is steadily increasing, with approximately 20 million intravenous administrations of radiopharmaceuticals occurring each year in the United States.[1] The most commonly used radiotracer in positron emission tomography (PET) imaging is 2-[^{18}F]fluoro-deoxy-D-glucose (^{18}F-FDG), a glucose analog employed to visualize abnormal metabolic activity associated with various diseases, including epilepsy, infection, Alzheimer's disease, heart disease, and other malignancies.[2] Besides ^{18}F-FDG, other commonly used radionuclides in PET imaging include ^{68}Ga and ^{89}Zr, while ^{99m}Tc is frequently used in single photon emission computed tomography (SPECT) imaging. To promote the safe use of these radiopharmaceuticals in medical applications, it is critical to understand and quantify the risks posed by the radioisotope and its intended application. One such concern in nuclear medicine is extravasation during the radiopharmaceutical injection.[3,4]

Extravasation refers to the accidental leakage of a radiopharmaceutical from a vein into the surrounding tissue during the course of an injection. The extent of the harm resulting from extravasation depends on several factors, such as the specific radiopharmaceutical involved, the administered activity, and the location and severity of the extravasation. Reports of radiopharmaceutical extravasation and/or infiltration have been documented as early as 1984,[5] with subsequent studies published thereafter.[6,7] Initially, it was assumed that radiopharmaceutical extravasation caused no physical harm to the patient during nuclear medicine procedures, and this assumption still appears to be valid.[8,9] The Society of Nuclear Medicine and Molecular Imaging (SNMMI) and American College of Nuclear Medicine (ACNM) have indicated that the additional absorbed doses resulting from radiopharmaceutical extravasation are not clinically significant.[10] However, there is a lack of publicly available data supporting this statement.

Recently published studies have claimed that radiopharmaceutical extravasation may have the potential to cause tissue damage at the local injection site.[11,12] Using MIRD techniques applied to real-time measurement of extravasation kinetics, Osborne et al. estimated that the absorbed doses at the site of extravasation could reach as high as 11.2 Gy in a tissue volume of 5 cm^3 with this work recently validated independently by Tsorxe and Hayes for the assumed extravasation volumes.[11–13] From a radiation safety perspective, the absorbed doses at the local site of extravasation may surpass the limits defined for medical events. Consequently, there is an interest in determining whether these occurrences should be classified as medical events. The Nuclear Regulatory Commission (NRC) has recently sought public comments on reporting nuclear medicine injection extravasations as medical events.[14] A recent Monte Carlo estimate by Sunderland et al. reported that the infiltration of an entire 10 mCi clinical injected activity of ^{18}F-FDG during PET imaging is unlikely to result in deterministic skin injury when taking into account skin tissue sub-anatomy where the fibrous dermal layer effectively shields the radiation sensitive epidermis from positron energy deposition.[15] This study looked at single time points at 1 h or more post-injection and used a combined 30-min biological/physical half-life for reabsorption based upon the work of Osborne et al.[11]

This raises the question of whether the accumulation of radiopharmaceuticals at the local injection site, specifically the extravasation of activity during diagnostic (PET or SPECT) imaging or therapeutic procedures, poses long-term harm. In particular, how much damage does it cause to the local extravasation site and underlying tissue? The work by Sunderland et al. used MCNP Monte Carlo simulations to estimate radiation absorbed dose to skin sub-anatomies (epidermis, dermis, subcutaneous tissue, and muscle) for several radionuclides and geometries, but did not extend their work to the cellular and DNA dose level. To shed light on these important concerns, this study employs advanced Monte Carlo simulations to replicate clinical extravasation scenarios and assess radiation damage resulting from extravasation. Monte Carlo techniques have become the preferred tool for describing radiation transport through matter. To comprehend the radiation's impact on cells at the injection site, we developed a Monte Carlo model replicating a clinical extravasation event and estimated the resulting radiation damage. The damage estimation was performed at the cellular level both at the site of extravasation as well as to other vital organs in the body.

The existing literature lacks reports on the organ-level dosimetric contribution arising from radiopharmaceutical extravasation. It is important to understand the contribution of extravasated activity to organ-level absorbed doses in order to fully comprehend the effects of extravasation around the injected area for both the patient and for those that could be in close proximity to the patient following an extravasation event (e.g., patient holding a child after diagnostic radiopharmaceutical extravasation). Therefore, this study aims to quantify the absorbed organ dose contribution from radiopharmaceutical extravasation by conducting Monte Carlo simulations on XCAT phantoms[16,17] using the Geant4 Application for Tomographic Emission (GATE) toolkit.[18,19] Moreover, skin-level dosimetry calculations were performed and absorbed doses were simulated at the epidermis, dermis, and hypodermis. To assess radiation damage, this work evaluates the likelihood of DNA damage resulting from the decay of ^{18}F and ^{68}Ga at the local extravasation site. Radiobiological effects, such as the extent of DNA damage in terms of DSBs and SSBs, were estimated using the TOPAS-nBio Monte Carlo platform.[20,21]

2 | MATERIALS AND METHODS

We used a multi-scale simulation approach in this work developed previously in our group.[22] Simulations were conducted using a validated Monte Carlo simulation pipeline developed at ORNL.[23] Macroscopic dosimetry simulations were performed using the GATE Monte Carlo platform,[18,19] which accurately captures realistic radiation fields for precise radiation dosimetry. In addition, cell-scale simulations involving the scoring of DNA damage in selected cells were performed using the Geant4[24] and TOPAS-nBio toolkits.[20,21] This comprehensive approach allowed us to analyze particle tracks and evaluate DNA damage at a cellular level, complementing the macroscopic dosimetry simulations.

2.1 | Organ level absorbed dose simulations

The GATE Monte Carlo toolkit was chosen for organ-level dosimetry, which we previously validated for radiopharmaceutical therapy dosimetry[25–27] along with XCAT phantoms from Duke University.[16] GATE is a Monte Carlo simulation code that incorporates the Geant4 libraries.[18,19,28,29] For this study, GATE version 9.1 was used to simulate XCAT phantoms, which closely represent the anatomy and physiology of clinical patients. Specifically, we employed the male XCAT phantom, with a height of 1.77 m, and weight of 72 kg, to represent the average adult male. The simulations involved estimating absorbed doses at the local extravasation site (injection location) and in various organs of the XCAT phantom, including the heart ($\rho = 1.05$ g/cm^3), gonads ($\rho = 1.04$ g/cm^3), liver ($\rho = 1.06$ g/cm^3), lungs ($\rho = 0.26$ g/cm^3), spleen ($\rho = 1.06$ g/cm^3), and kidneys ($\rho = 1.05$ g/cm^3).

The standard version of the XCAT mesh phantom was generated using the XCAT software. Subsequently, the XCAT mesh phantom was imported into AutoCAD software to save each organ as a stereolithography (STL) file. These STL files were imported into the GATE software to simulate the organs of interest. To minimize simulation time, we excluded the simulation of organs located in the lower abdominal region, as shown in Figure 1.

An energy cut of ~10 keV was applied as a lower bound, corresponding to a range cut of ~1 cm in the phantom body ($\rho = 1.04$ g/cm^3). A positron source was used for all simulations. For electromagnetic interactions, we utilized the physics list *emstandard_opt4* along with the radioactive decay. To calculate the energy deposition at the organ level, the *doseActor* mechanism in GATE was used. This actor stored the energy deposition information separately for each organ. In all *doseActor* setups, a voxel size of $2 \times 2 \times 2$ mm^3 was utilized. The energy deposition map was then converted into absorbed dose, considering only the irradiated voxels for absorbed dose estimation.

2.2 | Skin dosimetry

In our study, we modeled skin anatomy using average tissue layer thickness values. Specifically, we set the epidermis thickness at 0.2 mm ($\rho = 1.1$ g/cm^3), the dermis thickness at 1.5 mm ($\rho = 1.1$ g/cm^3), a hypodermal layer (or subcutaneous tissue) thickness of 7 mm ($\rho = 0.95$ g/cm^3), and a muscle layer thickness of 2 cm ($\rho = 1.04$ g/cm^3), as illustrated in Figure 2. While these dimensions are representative of an average population, it is essential to note that actual values can vary significantly.

In our Monte Carlo model, we assumed activity extravasation in the hypodermal layer based on clinical data available from Tylski et al.[30] The extravasation volume was represented by a rectangle measuring $2.8 \times 2.8 \times 0.7$ cm^3, with a volume of 5.5 mL. This volume served as the source volume in our simulations. Subsequently, we estimated absorbed doses for all tissue layers. Additionally, we separately estimated the contributions to the absorbed dose from positrons, electrons, and gammas through simulations.

2.3 | Choice of radionuclides

Two radionuclides were used in this work: ^{18}F and ^{68}Ga, with half-lives of 109.77 min and 67.71 min,

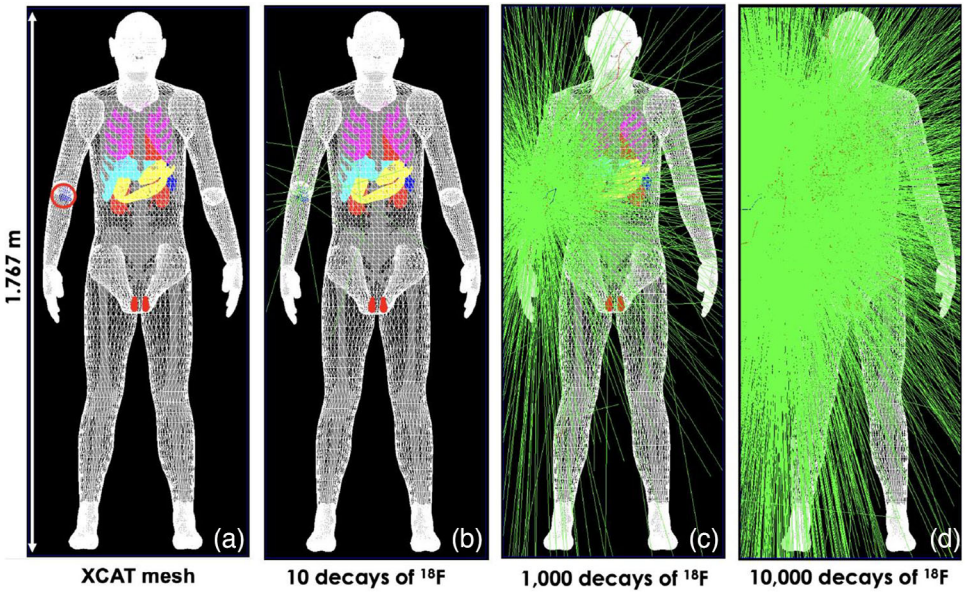

FIGURE 1 (a) XCAT male phantom visualization in GATE Monte Carlo platform, and (b–d) Visualization of ^{18}F decays in the antecubital fossa of the phantom's right arm. The green lines in the figure represent photon emissions from positron annihilation within the phantom.

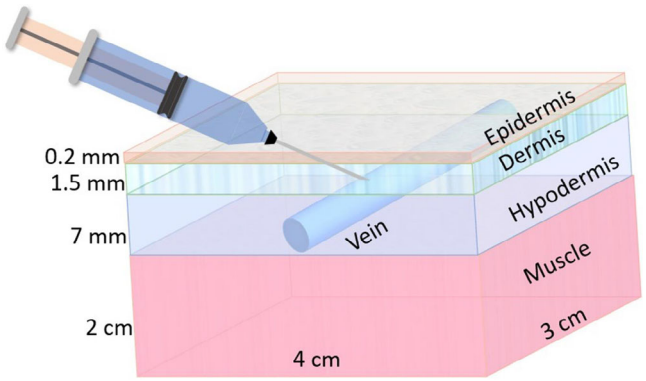

FIGURE 2 Schematic representation of the modeled skin anatomy for calculating absorbed doses at the skin level.

respectively.[31] After injecting the radiopharmaceutical, two processes occur internally: (1) radioactive decay of the nuclide in situ and (2) biological clearance of the radiopharmaceutical (i.e., wash out). For organ-level absorbed dose calculations, the first two half-lives were simulated for both radionuclides, representing 75% of their total decay, providing a conservative and safe estimate. The remaining 25% was assumed to be biologically cleared from the XCAT phantom, mimicking realistic clinical conditions. The assumption of 25% clearance was based on the biological half-life of ^{18}F, which is ~1 h, resulting in an effective half-life of ~33 min.[11]

When ^{18}F decays, it releases positrons (96.7%) with an average energy (E_{ave}) of 249 keV. The subsequent annihilation of these positrons with electrons produces annihilation photons (γ-rays) with an energy of 511 keV.[31] In clinical settings, the injected activity of ^{18}F-FDG can vary, but a typical clinical scan often employs an activity of 10 mCi of ^{18}F-FDG. In this study, we assumed that 10% of the activity of ^{18}F (i.e., 1 mCi) was extravasated in the antecubital fossa of the right arm of the XCAT phantom. Our assumption was based on realistic cases of extravasation observed in clinical settings and aligns with the majority of cases reported in the literature.[12] To estimate organ-level dosimetry, a total of 263.73 billion ^{18}F decays were simulated to account for the level of extravasated activity.

^{68}Ga is also a positron emitter, decaying 89% through positron emission, with an average energy (E_{ave}) of 836 keV and a maximum energy of 1.92 MeV.[31] The positron emission energy is higher compared to ^{18}F. This radionuclide has a shorter half-life and a faster clearance time compared to ^{18}F. A typical injected activity of ^{68}Ga-DOTATATE in clinics is ~5 mCi. Assuming 10% extravasation, we simulated an extravasated activity of 0.5 mCi, corresponding to a total of 81.34 billion decays of ^{68}Ga.

All of these simulations were performed on the CADES computing cluster at Oak Ridge National Laboratory. Parallel simulations were executed to reduce the overall computing time, and the output files were summed after simulations for further analysis.

2.4 | Radiobiology simulations

Radiobiology simulations were performed to understand whether the energy deposition from positron (β^+) and gamma (γ) emissions resulting from annihilation would cause damage to DNA strands and to assess the extent of this damage. The extravasated volume was modeled

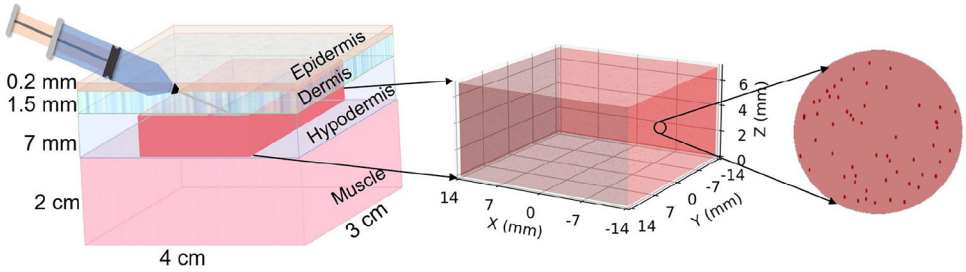

FIGURE 3 Geometry of the homogeneous extravasation rectangular volume used in the right arm of the XCAT phantom (shown in red). The enlarged portion of the figure shows cells randomly suspended in a radioactive solution of ^{18}F. Phase space files for each cell were generated from the Geant4 simulation.

as a homogeneous rectangular tissue volume placed in the right arm of the XCAT phantom, as shown in Figure 1. The number of DSBs and SSBs in the nuclear DNA was estimated using the TOPAS-nBio (version 2.0) Monte Carlo simulation toolkit. This toolkit wraps and extends the general-purpose Monte Carlo Geant4 code and provides detailed track structure simulations of physics and chemistry down to vibrational energies (~2 eV) within realistic biological systems.[20,21] Moreover, TOPAS-nBio offers an extensive library of biological geometries, encompassing various scales ranging from micrometers (e.g., cells and sub-cellular structures) to nanometers (e.g., DNA molecules and proteins).

2.4.1 | Geant4 simulation setup

The simulated extravasated volume of 5.5 mL was designed to contain 2000 randomly spaced spherical cells with a diameter of 20 μm, each containing a nucleus with a diameter of 10 μm. All cells and nuclear volumes were spherical in shape. It is important to note that the simulation did not take account the cell cycle, its stages, or the variations in cellular morphologies. Additionally, all cells and the entire extravasation volume were composed of water ($\rho = 1$ g/cm^3).

The Geant4 simulation was employed to estimate the number, types, and energies of particles upon their entry into the cell nucleus. Figure 3 illustrates the simulation of the extravasation rectangular volume with randomized cells, conducted in Geant4 (*geant4-10-07-patch-03*) before the TOPAS-nBio simulations. The number of cells was selected to minimize the computation time while also providing sufficient statistical variation in the output. The volumetric *GenericIon* source was used in the Geant4 simulation for both ^{18}F and ^{68}Ga. The simulation included the radioactive decay process in the physics list, along with *G4EmStandardPhysics_option4*. Additionally, the Livermore low-energy physics model was incorporated, as this model is valid for energies down to 100 eV.[32] Atomic de-excitation processes such as Auger cascades and fluorescence were also included in the simulations. From the Geant4 simulations, phase space data of particles entering the nucleus were recorded. Phase space files were generated for all randomized cells, capturing the position, energy, particle types, and direction cosines of the particles within the nuclear volume. These files were subsequently used as a source in the TOPAS-nBio simulations.

2.4.2 | TOPAS-nBio simulation

As with the absorbed organ dose calculations, two radionuclides were used in these simulations: ^{18}F and ^{68}Ga. The DNA damage resulting from exposure to these radionuclides, measured in terms of DSBs and SSBs, was simulated using TOPAS-nBio. The TOPAS-nBio simulations were essentially single-cell simulations. We employed phase space files derived from Geant4 as a source within TOPAS-nBio, as illustrated in Figure 4. To simulate the physics and chemistry processes, *g4em-dna* and *emDNAChemistry* modules were enabled. We used a generic cell nucleus model consisting of the human genome defined by Zhu et al.[33] In TOPAS-nBio simulations, a direct DNA strand break was scored when the accumulated energy deposition exceeded 11.5 eV within the backbone volume and its surrounding hydration shell in a single history. For chemically induced indirect DNA damage simulations, we used water radiolysis products which are available as the default chemistry reactions in TOPAS-nBio. Further details on the chemistry stage reactions are available elsewhere.[34] Breaks occurring in the sugar-phosphate backbone on opposite strands of the DNA helix, within a maximum separation of 1 helical turn (~10 base pairs),[35,36] were classified as DSBs, while breaks occurring elsewhere were considered SSBs.[33] The yields of DSBs and SSBs are reported as the number of breaks per nucleus.

To minimize statistical uncertainties, higher statistics or a larger number of decays were employed in the Monte Carlo simulations for all scenarios. A total of 10 simulations were conducted for each scenario to

TABLE 1 Organ-level dosimetry using the XCAT phantom with ^{18}F and ^{68}Ga radionuclides with 10% extravasation.

Number	Organs	^{18}F-radionuclide Absorbed dose (μGy)	^{68}Ga-radionuclide Absorbed dose (μGy)
1	Heart	7.53 ± 0.05	27.49 ± 0.25
2	Right gonad	3.01 ± 0.02	1.79 ± 0.34
3	Left gonad	2.26 ± 0.04	1.45 ± 0.20
4	Liver	753.10 ± 6.01	574.92 ± 5.14
5	Right lung	37.75 ± 0.30	38.27 ± 0.36
6	Left lung	11.30 ± 0.10	13.99 ± 0.19
7	Spleen	1.88 ± 0.01	6.42 ± 0.09
8	Right kidney	75.32 ± 0.51	96.42 ± 0.94
9	Left kidney	3.01 ± 0.02	4.82 ± 0.05

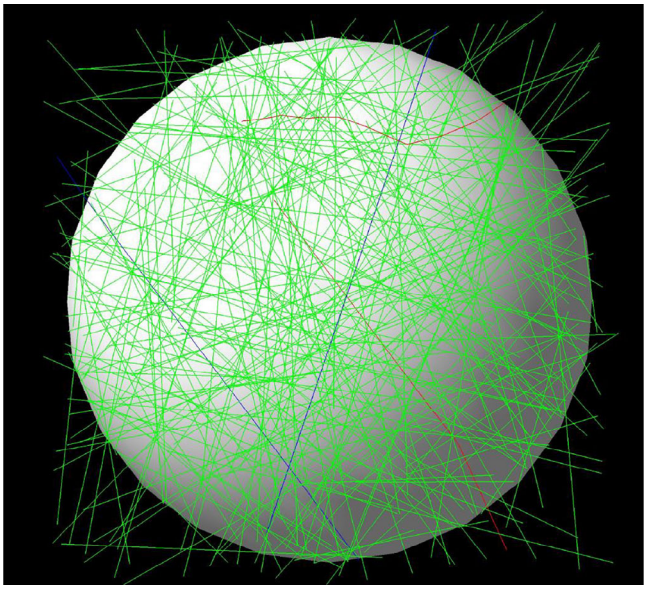

FIGURE 4 Illustration of the simulation of a phase space source obtained using Geant4 (using 1 billion decays of ^{18}F) in TOPAS-nBio. Green lines represent gammas, red lines denote electrons, and blue lines are positron tracks in a nuclear volume. Please note that the full details of the nucleus geometry are not visualized in the figure.

determine the average, standard deviation, and coefficient of variation in the absorbed dose, DSBs, and SSBs per nucleus.

3 | RESULTS

3.1 | Organ level absorbed dose simulations

The absorbed dose estimations at the organ level were obtained from the GATE simulations. Table 1 presents the absorbed dose estimates for various organs using 1 mCi (37 MBq) of ^{18}F and 0.5 mCi (18.5 MBq) of ^{68}Ga within an extravasated rectangular volume, using the standard male XCAT phantom. Absorbed doses to the extravasation site will be discussed in the subsequent section along with detailed information. The tabulated absorbed dose deposition in all organs pertains solely to gamma photon absorbed doses.[37,38]

3.2 | Skin dosimetry

Considering a 10% activity extravasation of ^{18}F and ^{68}Ga radionuclides, we observed that the hypodermal layer of the skin received the highest dose: 1.32 ± 0.01 Gy for ^{18}F and 0.99 ± 0.01 Gy for ^{68}Ga. Similarly, the epidermal and dermal layers received absorbed doses of 0.07 ± 0.01 Gy and 0.13 ± 0.01 Gy for ^{18}F, and 0.14 ± 0.01 Gy and 0.29 ± 0.01 Gy for ^{68}Ga, respectively. Additionally, the muscle layer received a comparable absorbed dose of 0.04 ± 0.01 Gy for both radionuclides. These results are summarized in Figure 5a,b. The Monte Carlo uncertainties in these skin dosimetry results were all less than 2%.

At the extravasation site (located in the hypodermal layer), where there was 10% extravasation of the radiotracer, the simulations with ^{18}F resulted in a total absorbed dose of 1.56 ± 0.02 Gy. Similarly, simulations with the ^{68}Ga radionuclide yielded a total absorbed dose of 1.46 ± 0.03 Gy. The simulated absorbed doses at the extravasation site are primarily due to positrons as shown in Figure 5b.

Figure 5b illustrates the dosimetric contributions of each particle type in the hypodermal layer, where the absorbed dose is highest. Our findings suggest that with 100% extravasation, assuming an identical volume, the hypodermis would receive over 13 Gy using ^{18}F and 10 Gy using ^{68}Ga, while the epidermis would receive less than 1.4 Gy of absorbed doses. The lower absorbed doses observed at the epidermis indicate that the dermal layer serves as a shield for positrons, thus minimizing the absorbed doses in the epidermis. This observation is consistent with prior research by Sunderland et al.[15]

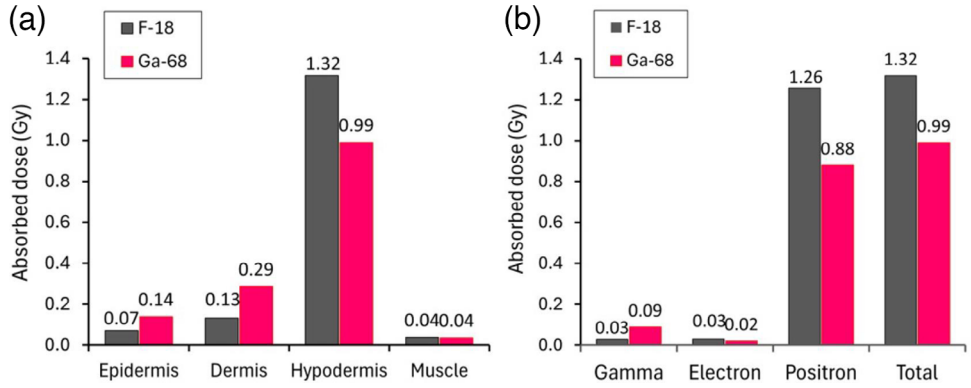

FIGURE 5 (a) Absorbed doses across different skin layers, and (b) Contributions of different particles to absorbed doses in the hypodermal layer of the skin.

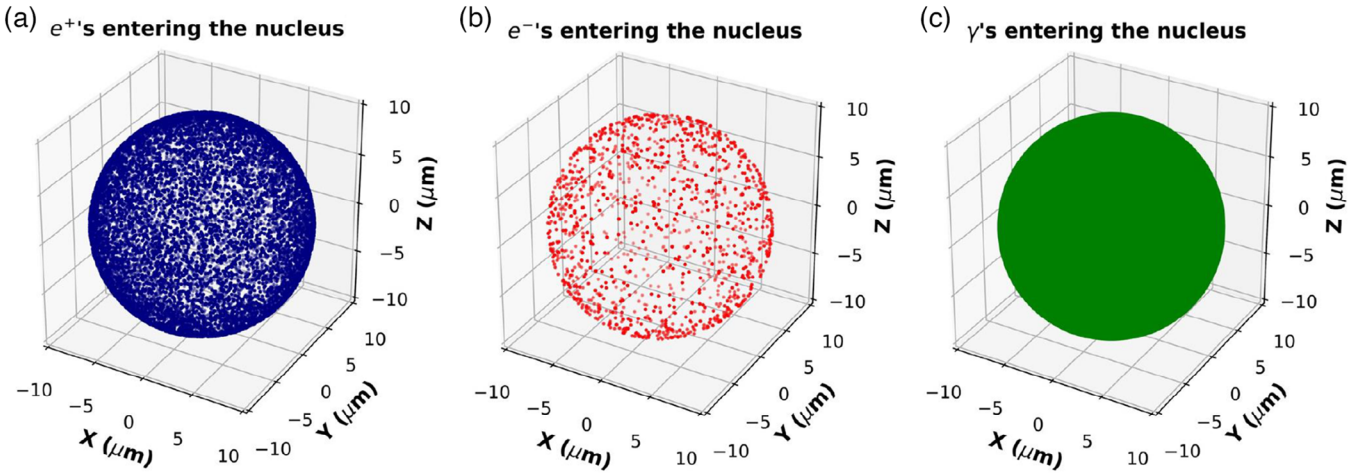

FIGURE 6 Positions of the particles entering the nucleus of a single cell using 263.73 billion decays of ^{18}F. Positions of the (a) positrons, (b) electrons, and (c) gammas entering the nucleus. A large number of gammas entered the nuclear volume compared to positrons and electrons (indistinguishable green dots in sub-figure c).

3.3 | Radiobiology simulations

3.3.1 | Geant4 simulation

The decay of ^{18}F results in the emission of different types of particles that penetrate nuclear volumes, including positrons, electrons, and γ-rays, each with varying energy levels. Figure 6 provides a summary of the positions of particles entering a single-cell nuclear volume. Please note that we ignored the neutrinos resulting from the β^+-decay of ^{18}F. On average, out of 263.73 billion decays of ^{18}F, approximately 11,454 ± 176 (±1.54%) positrons, 1,265 ± 25 (±2.01%) electrons, and 268,290 ± 445 (±0.17%) γ-rays entered the nucleus. The probability of these particles reaching the nucleus was found to be significantly influenced by the nuclear diameter. The electrons that enter the nucleus are secondary electrons generated through ionization caused by the interactions of positrons and γ-rays with the extravasation volume. As expected, Figure 7c demonstrates a significant influx of gamma photons with an energy of 511 keV into the nuclear volume.

Similarly, as shown in Figure 8, nuclear volumes are penetrated by positrons, γ-rays, and secondary electrons resulting from the radionuclide decay of ^{68}Ga. The figure provides an average breakdown of the contributions made by each particle type to the nucleus. On average, out of 81.34 billion ^{68}Ga decays, approximately 17,792 ± 1,090 (±6.13%) positrons, 768 ± 26 (±3.44%) electrons, and 72,429 ± 274 (±0.38%) γ-rays enter a nuclear volume. Interestingly, despite the lower number of ^{68}Ga decays, Figure 9a illustrates a higher influx of positrons into the nucleus compared to ^{18}F decays. Regarding γ-rays, the majority consists of 511 keV photons, while a small fraction comprises low-energy photons, as shown in the inset of Figure 9c.

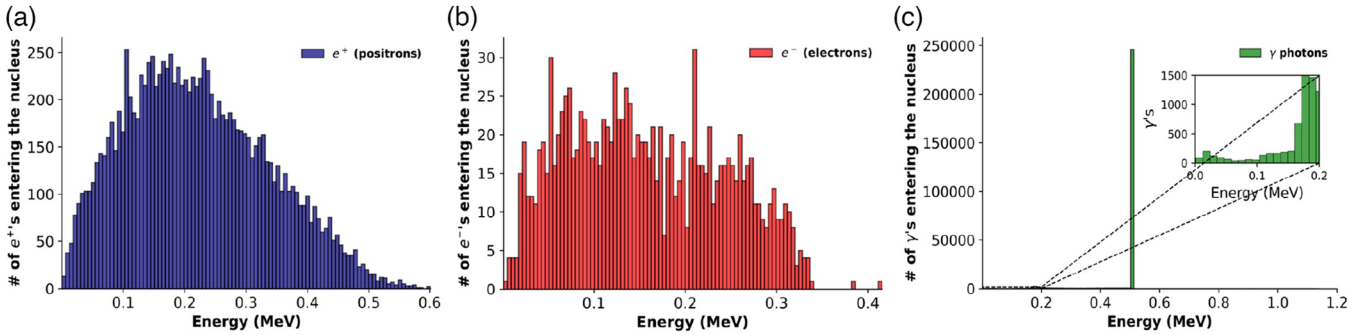

FIGURE 7 Energy spectra of different types of particles entering a cell nuclear volume using 263.73 billion decays of ^{18}F: (a) positrons, (b) electrons, and (c) gammas.

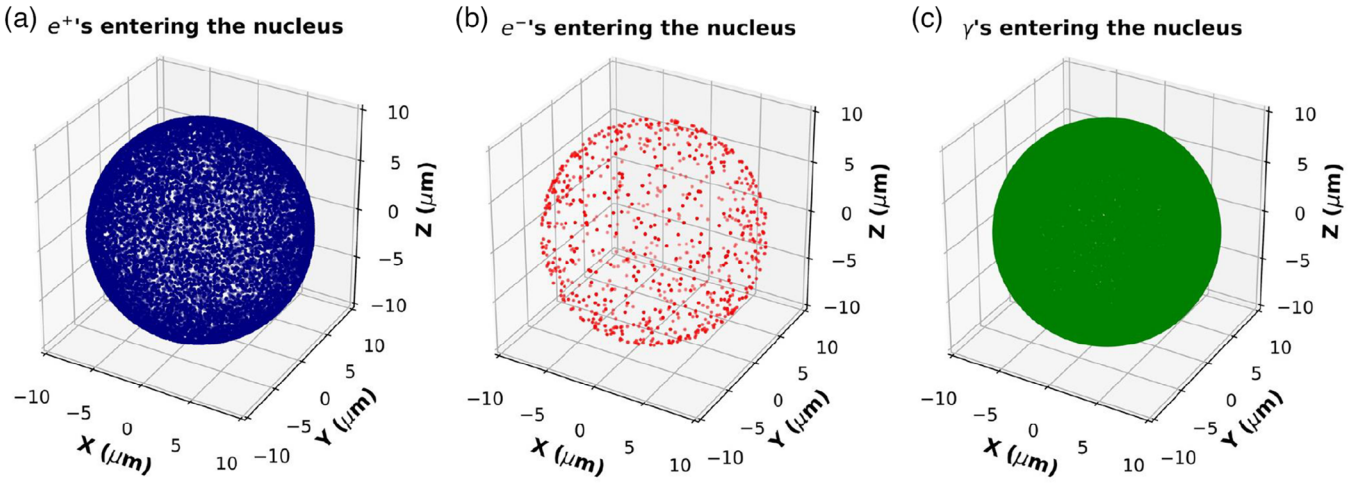

FIGURE 8 Positions of the particles entering a single cell nuclear volume using 81.34 billion decays of ^{68}Ga. Positions of the (a) positrons, (b) electrons, and (c) gammas entering the nucleus.

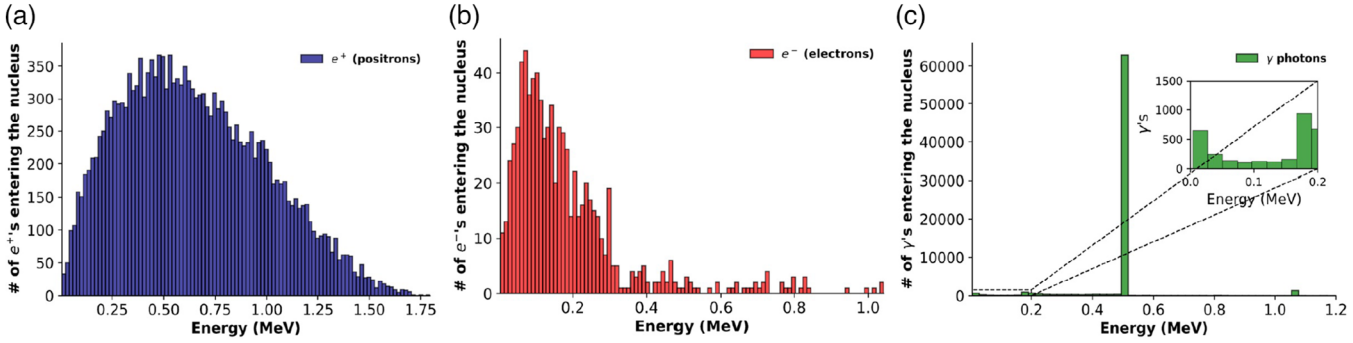

FIGURE 9 Energy spectra analysis of particle types entering a cell nuclear volume utilizing 81.34 billion decays of ^{68}Ga: (a) positrons, (b) electrons, and (c) gammas.

3.3.2 | TOPAS-nBio simulation

The discussion of results to this point has dealt with the analysis of phase space files from the Geant4 simulation. It is now time to present the results of the radiobiology simulations conducted using the TOPAS-nBio platform. Our evaluation focused on studying DNA strand breaks, specifically DSBs and SSBs, as well as the absorbed dose received by the cell nucleus. The extravasated rectangular volume contained a uniform source of ^{18}F and ^{68}Ga, leading us to expect a similar level of absorbed dose and DNA strand breaks

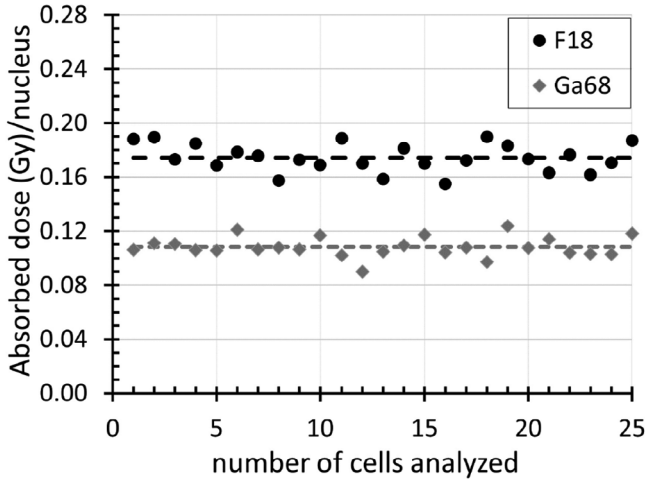

FIGURE 10 Absorbed dose per nucleus versus the number of cells analyzed for ^{18}F and ^{68}Ga decays. Dashed lines represent the average absorbed dose received by the nuclei.

throughout the volume. However, the absorbed dose should exhibit greater uniformity in the central region of the extravasated volume, as opposed to the region closer to the wall.

Figure 10 illustrates our findings, indicating a comparable level of absorbed dose per nucleus in the analyzed cells. These cells were located in the central region of the extravasated volume. Two dashed lines in Figure 10 represent the average absorbed dose per nucleus: 0.17 ± 0.01 Gy/nucleus for ^{18}F simulations and 0.11 ± 0.01 Gy/nucleus for ^{68}Ga simulations conducted within the extravasated volume containing cellular volumes. These values correspond to the coefficient of variations of 5.74% and 6.48% for ^{18}F and ^{68}Ga, respectively.

In Figure 11a,b, we depict the quantity of DNA DSBs per nucleus within the analyzed cells. On average, from the decay of ^{18}F in the extravasated volume, we observed 3.51 ± 0.27, 7.08 ± 0.29, and 10.58 ± 0.50 DSBs per nucleus, categorized as direct, indirect, and total DSBs per nucleus, respectively. Similarly, from the decay of ^{68}Ga, we observed 2.15 ± 0.21, 4.35 ± 0.20, and 6.49 ± 0.34 direct, indirect, and total DSBs per nucleus. The coefficient of variation for DSBs per nucleus was 7.71%, 4.06%, and 4.73% for direct, indirect, and total DSBs using ^{18}F, respectively, 9.93%, 4.68%, and 5.18% when utilizing ^{68}Ga.

The simulated results for SSBs per nucleus are presented in Figure 12a,b. Figure 12a provides data on direct, indirect, and total SSBs per nucleus. The simulated average values for ^{18}F decays in the extravasated volume are as follows: direct SSBs per nucleus, 98.67 ± 5.92; indirect SSBs per nucleus, 169.44 ± 7.09; total SSBs per nucleus, 268.11 ± 12.43. In contrast, for ^{68}Ga decays, the levels of SSBs per nucleus are lower compared to ^{18}F, with average values of 59.23 ± 4.05, 102.01 ± 4.91, and 161.24 ± 8.12, respectively.

The coefficient of variation for SSBs per nucleus was 6.01%, 4.18%, and 4.64% for direct, indirect, and total SSBs using ^{18}F, respectively, and 6.84%, 4.81%, and 5.03% when utilizing ^{68}Ga. We observed similar levels of variability for both types of DNA damage. This variability can be attributed to the limited number of particles reaching cellular volumes, as depicted in Figures 6 and 8. However, this level of variability was considered acceptable for the current study.

In both simulations involving ^{18}F and ^{68}Ga sources, the contribution of the gamma photons to the occurrence of DSBs and SSBs was negligible (< 1%). This is due to the fact that gamma rays lack charge, making them less likely to interact directly with electrons in the atom. Additionally, Figures 7c and 9c visually depict the limited number of low-energy gammas entering the nuclear volume (refer to insets). Instead, the primary source of DNA damage was positrons. The number of positrons was significantly higher than the number of secondary electrons generated during the interactions.

4 | DISCUSSION

In this study, we present the first detailed investigation of extravasation in PET imaging using Monte Carlo simulations that consider radiobiological factors. Our research focused on two main aspects: (1) estimating the absorbed dose at the local injection site and in other proximal organs due to extravasation, and (2) assessing the extent of DNA damage, specifically DSBs and SSBs, at the local injection site.

Through our simulations, we estimated that the absorbed dose at the injection site (the patient's right arm tissue), resulting from extravasation ranging from 10% to 100% (worst-case scenario), ranged from 1.56 to 15.6 Gy for ^{18}F and 1.46 to 14.6 Gy for ^{68}Ga. However, these values represent the cumulative absorbed doses across the three layers of the skin. Specifically, the absorbed dose in the epidermis, which influences erythema, ranged from 0.14 Gy to 1.4 Gy for ^{18}F and 0.07 Gy to 0.7 Gy for ^{68}Ga in the worst-case scenario. Notably, these values remain well below the thresholds associated with skin erythema. A commonly referenced threshold for deterministic effects, such as skin epidermal erythema, to manifest due to ionizing radiation typically ranges between 2 and 6 Gy.[39,40] Our simulated absorbed dose at the epidermis remained below 2 Gy, even under conditions of 100% extravasation, suggesting a low risk of skin epidermal erythema and desquamation.

It is important to note that these referenced thresholds are primarily derived from external beam radiation therapy. Given the early stage of dosimetry data for radiopharmaceutical administrations and the absence of specific dose-response information for erythema, comparisons with existing literature are limited. In

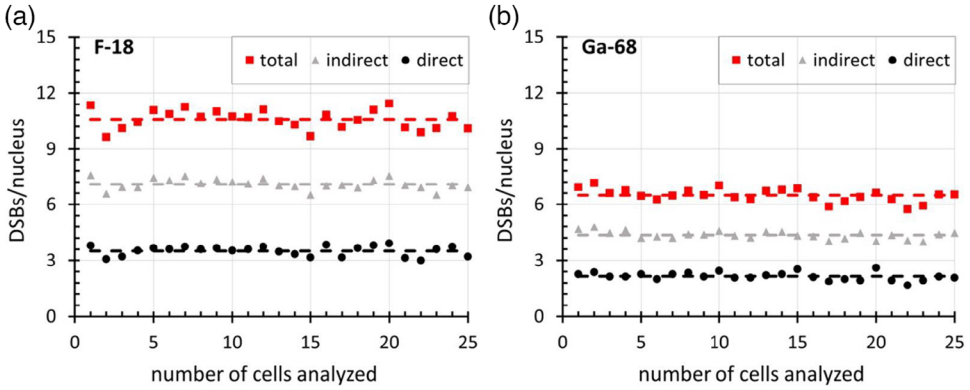

FIGURE 11 DNA DSBs induced by the decay of ^{18}F and ^{68}Ga. (a) Contributions of direct and indirect DSBs per nucleus in multiple cells resulting from ^{18}F decay, and (b) comparison of DSBs per nucleus from ^{68}Ga decay across multiple cells. All of the analyzed cells were located in the central region of the rectangular volume. Dashed lines indicate the average number of DSBs incurred by the nucleus.

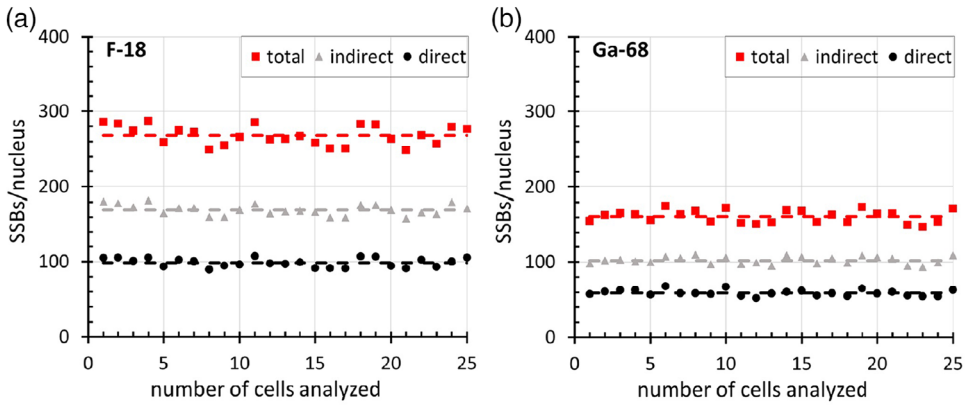

FIGURE 12 (a) SSBs per nucleus resulting from the decay of ^{18}F, and (b) SSBs per nucleus arising from the decay of ^{68}Ga within the extravasated rectangular volume. Dashed lines represent the average number of SSBs suffered by the nucleus.

a worst-case scenario, the hypodermal layer could receive more than 13 Gy using ^{18}F and 10 Gy using ^{68}Ga. Such absorbed doses may induce toxicity in the deeply infiltrated hypodermal layers. However, the hypodermis is less radiosensitive, less cellular, and has low proliferative capacity compared to the epidermis and dermis, reducing the likelihood of significant toxicity. Nevertheless, literature on the impact of higher absorbed doses in subdermal layers is scarce, making it challenging to predict deterministic effects in these tissues. This underscores the necessity for further research to understand the potential effects of absorbed doses in deeper tissue layers.

Moreover, higher absorbed doses in the hypodermis may not result in visible manifestations. This challenges the assumption that visible skin effects can reliably indicate the severity of extravasation. The absence of skin effects does not necessarily mean that deeper layers are unaffected. Therefore, alternative methods must be considered to accurately assess the severity of extravasations, particularly those involving high activities of radiopharmaceuticals.

Our simulated values for the epidermis are significantly lower than the absorbed dose estimates of 11 Gy reported by Osborne et al. and Tsorxe-Hayes.[11,13] Despite their use of similar extravasated volume (5 mL) in their work, the discrepancy is primarily attributed from differences in the geometry of extravasated volumes. Specifically, they estimated the skin absorbed dose for a contiguous 10 cm^2 area of skin at a tissue depth of 70 μm where our current study segmented this larger region of tissue into appropriate sub-compartments. Further biological modeling studies can also help show that, even though classical calculation of absorbed dose levels can be higher, the detriment to the patient for diagnostic radiopharmaceuticals is likely negligible due to varying radiation sensitivities of even closely oriented tissues.

The organ-level dosimetry calculations are reported in Table 1. The absorbed dose estimates for organs using both ^{18}F and ^{68}Ga fell within the micro-gray (μGy) range, corresponding to an equivalent dose on the order of micro-Sieverts (μSv) when considering a radiation weighting factor of one for both γ and β-particles (β^+

and β^-), indicating their insignificance. These findings support the statement made by professional societies representing the interests of nuclear medicine practitioners, such as SNMMI and ACNM. These societies assert that absorbed doses at the organ-level resulting from extravasation are clinically insignificant.[10]

Please note that the extravasation volume used in this work was estimated using imaging data from recent publications by Tylski et al.[30] and Osborne et al.[12] We selected a modeled volume to simplify Monte Carlo simulations, representing realistic clinical situations by assuming a 10% extravasation, as typically observed in clinical settings.[12] Moreover, our study quantified the DNA damage caused by the ^{18}F and ^{68}Ga radiotracers and determined whether extravasation posed any harm at the cellular level. By simulating a simple extravasation model consisting of randomly oriented cells with nuclear DNA using the TOPAS-nBio toolkit, we found that irradiating extravasated activity at the local site produced a total of 10.58 $\pm$ 0.50 DSBs/nucleus on average using ^{18}F and a total of 6.49 $\pm$ 0.34 DSBs/nucleus with ^{68}Ga. In addition, 268.11 $\pm$ 12.43 SSBs/nucleus were estimated from the decay of ^{18}F and 161.24 $\pm$ 8.12 SSBs/nucleus arising from the decay of ^{68}Ga in the extravasated volume. All of these DNA damage calculations were estimated in the hypodermal layer of the skin. From Figure 5a, we observed that the epidermis received only 0.07 Gy for ^{18}F, which is approximately 20 times less than the hypodermal absorbed dose. Presumably, given the significant absorption of positrons in the hypodermis and dermis, we can expect a significantly lower proportion of DNA DSB in the epidermal layer of the skin. It is important to note that this estimation was based on the assessment of cells with the same cellular morphologies and the simulation model employed a generic cell and nucleus model.

Our study was not without limitations. A major limitation of our study was the omission of DNA repair simulation following strand breaks. Specifically, our simulation did not account for whether the simulated DSBs and SSBs underwent any repair after radiation exposure from the decay of ^{18}F and ^{68}Ga. Existing literature suggests that the repair mechanism depends on various factors, including cell type, extent of damage, and available repair pathways within the cell.[41,42] SSBs are generally easier to repair than DSBs. Unrepaired or misrepaired DSBs can have detrimental effects on cellular function, leading to cell death, and genomic instability, and potentially contributing to the development of diseases, including cancer. However, the number of DSBs resulting from the decay of both ^{18}F and ^{68}Ga decays was found to be fewer than eleven DSBs per cell using 10% extravasation of activity (1 mCi for ^{18}F and 0.5 mCi of ^{68}Ga) in the antecubital fossa of the right arm of the XCAT phantom. The simulated DSBs are comparable to those reported in the literature for background radiation for somatic cells (the non-reproductive cells of the human body). Literature reports that DSBs are consistently generated in metabolically active cells due to background radiation, with the number ranging from 10 to 50 DSBs per cell per day, depending on the cell cycle stage and tissue type.[43,44] These DBSs are continuously repaired to maintain genomic stability. Therefore, it is likely that the DSB damage caused by ^{18}F and ^{68}Ga will be repaired and pose no long-term adverse risk.

In summary, we successfully employed Monte Carlo simulations to measure organ-level absorbed doses based solely on extravasation and potential biological effects. However, we acknowledge certain challenges in accurately predicting DNA damage, such as incorporating variations in cellular morphologies, cell types associated with the extravasation volume, and cell cycle radiosensitivity. Additionally, in this study, we used a standard male XCAT phantom and considered only two radionuclides. In this study, we assumed a biological washout of 25%, disregarding the potential influence of radiotracer chemical forms on body clearance rates, which may impact dosimetry accuracy. Furthermore, we estimated the impact of extravasated activities on DNA damage using a homogeneous rectangular volume. These limitations highlight the importance of further research to incorporate these elements into our Monte Carlo model. Future studies should address these limitations to provide more accurate predictions, and this simulation framework can be used to assess the extravasation of therapeutic β- and α-emitting radiopharmaceuticals. Overall, our study provides valuable information regarding the dosimetry and potential biological effects of extravasation in PET imaging, contributing to the ongoing efforts to ensure safe and effective patient care in nuclear medicine PET imaging.

5 | CONCLUSION

In this study, we conducted comprehensive Monte Carlo simulations to investigate the effects of extravasation in PET imaging, considering both absorbed dose estimation in organs and assessment of DNA damage. This work enabled us to estimate absorbed doses both locally and in other organs such as the liver and kidneys from extravasation at a specific site in the body. Our findings indicated that the absorbed dose resulting from extravasation in the patient's arm is on the order of one gray (Gy), while absorbed doses in organs fall within the micro-gray (μGy) range. These findings support the conclusion that extravasation-related absorbed doses are not clinically significant at the organ level. Further, our simulation results indicate that the absorbed dose resulting from extravasation in PET imaging is unlikely to cause epidermal erythema, as the simulated absorbed

doses to the epidermis remain below the threshold known to trigger such effects.

In the worst-case scenario, the hypodermis might receive absorbed doses of around 13 Gy. However, this level of absorbed dose is less likely to lead to the deterministic effects in that layer. Moreover, the radiobiology simulations demonstrated minimal DNA damage in terms of DSBs at the extravasation site, implying that no long-term harm, such as radiation-induced carcinogenesis, should be expected.

ACKNOWLEDGMENTS

This work was supported by the Department of Energy (DOE)'s Office of Biological and Environmental Research (BER), Biological Systems Science Division (BSSD), and Laboratory Directed Research and Development Program of Oak Ridge National Laboratory, managed by UT-Battelle, LLC, for the U.S. Department of Energy. This research used resources from the Compute and Data Environment for Science (CADES) at the Oak Ridge National Laboratory. This manuscript has been authored by UT-Battelle, LLC under Contract No. DE-AC05-00OR22725 with the U.S. Department of Energy.

CONFLICT OF INTEREST STATEMENT

The authors have no relevant conflicts of interest to disclose.

DATA AVAILABILITY STATEMENT

The GATE scripts for Monte Carlo simulations of the XCAT phantom can be found on GitHub: https://github.com/ashok-tiwari. Other datasets generated and analyzed are available from the corresponding author upon reasonable request.

REFERENCES

1. National Research Council (US) and Institute of Medicine (US) Committee on State of the Science of Nuclear Medicine. *Advancing Nuclear Medicine Through Innovation*. National Academies Press (US); 2007. doi: 10.17226/11985
2. Rohren EM, Turkington TG, Coleman RE. Clinical applications of PET in oncology. *Radiology*. 2004;231(2):305-332.
3. Osborne DR, Acuff SN, Fang M, Weaver MD, Fu Y. Assessing and reducing PET radiotracer infiltration rates: a single center experience in injection quality monitoring methods and quality improvement. *BMC Med Imaging*. 2020;20(1):3.
4. Wong TZ, Benefield T, Masters S, et al. Quality improvement initiatives to assess and improve PET/CT injection infiltration rates at multiple centers. *J Nucl Med Technol*. 2019;47(4):326-331.
5. Castronovo F, McKusick K, Strauss H. Dosimetric implications of the infiltrated injection. *J Nucl Med;(United States)*. 1984;25(CONF-840619-).
6. Castronovo FP Jr, McKusick KA, Strauss HW. The infiltrated radiopharmaceutical injection: dosimetric considerations. *Eur J Nucl Med*. 1988;14(2):93-97.
7. Larson DL. What is the appropriate management of tissue extravasation by antitumor agents?. *Plast Reconstr Surg*. 1985;75(3):397-405.
8. van der Pol J, Vöö S, Bucerius J, Mottaghy FM. Consequences of radiopharmaceutical extravasation and therapeutic interventions: a systematic review. *Eur J Nucl Med Mol Imaging*. 2017;44(7):1234-1243.
9. Parihar AS, Schmidt LR, Crandall J, Dehdashti F, Wahl RL. Adverse Clinical events at the injection site are exceedingly rare after reported radiopharmaceutical extravasation in patients undergoing ^{99m}Tc-MDP whole-body bone scintigraphy: a 12-year experience. *J Nucl Med*. 2023;64(3):485-490.
10. Accessed Feb 10, https://www.regulations.gov/comment/NRC-2020-0141-0428 2023.
11. Osborne D, Kiser JW, Knowland J, Townsend D, Fisher DR. Patient-specific extravasation dosimetry using uptake probe measurements. *Health Phys*. 2021;120(3):339-343.
12. Osborne D, Lattanze R, Knowland J, et al. The scientific and clinical case for reviewing diagnostic radiopharmaceutical extravasation long-standing assumptions. *Front Med*. 2021;8:684157.
13. Tsorxe IY, Hayes RB. Dose estimation for extravasation of 177Lu, 99mTc, and 18F. *Health Phys*. 2023;124(3):217-220.
14. Federal Register. Reporting nuclear medicine injection extravasations as medical events. Federal Register; 2023. Accessed May 23. https://www.federalregister.gov/documents/2023/04/19/2023-08238/reporting-nuclear-medicine-injection-extravasations-as-medical-events
15. Sunderland JJ, Graves SA, York DM, Mundt CA, Bartel TB. Multicenter evaluation of frequency and impact of activity infiltration in PET imaging, including microscale modeling of skin-absorbed dose. *J Nucl Med*. 2023;64:1095-1101. doi:10.2967/jnumed.123.265891
16. Segars WP, Sturgeon G, Mendonca S, Grimes J, Tsui BM. 4D XCAT phantom for multimodality imaging research. *Med Phys*. 2010;37(9):4902-4915.
17. Segars WP, Mahesh M, Beck TJ, Frey EC, Tsui BM. Realistic CT simulation using the 4D XCAT phantom. *Med Phys*. 2008;35(8):3800-3808.
18. Sarrut D, Bardiès M, Boussion N, et al. A review of the use and potential of the GATE Monte Carlo simulation code for radiation therapy and dosimetry applications. *Med Phys*. 2014;41(6):064301.
19. Sarrut D, Bala M, Bardiès M, et al. Advanced Monte Carlo simulations of emission tomography imaging systems with GATE. *Phys Med Biol*. 2021;66(10):10.
20. McNamara A, Geng C, Turner R, et al. Validation of the radiobiology toolkit TOPAS-nBio in simple DNA geometries. *Phys Med*. 2017;33:207-215.
21. Schuemann J, McNamara AL, Ramos-Mendez J, et al. TOPAS-nBio: an extension to the TOPAS simulation toolkit for cellular and sub-cellular radiobiology. *Radiat Res*. 2019;191(2):125-138.
22. Inman P, Houri J, Gounley J, Agasthya G, Kapadia A. A computational multiscale framework for precision dosimetry in radiation therapy. *Med Phys*. 2022;49(6):E485-E485.
23. Tiwari A, Gonzalez MT, Andriotty MS, Agasthya GA, Kapadia AJ, Experimental validation of Monte Carlo simulations for quantifying DNA damage in breast cancer cells exposed to 225-Ac. Abstract presented at: 17th International Congress For Radiation Research 2023; Montreal, Canada.
24. Agostinelli S, Allison J, Amako K, et al. Geant4—a simulation toolkit. *Nucl Instrum Methods Phys Res A*. 2003;506(3):250-303.
25. Tiwari A, Sunderland J, Graves SA, Strand S, Flynn R. Absorbed dose distributions from beta-decaying radionuclides: experimental validation of Monte Carlo tools for radiopharmaceutical dosimetry. *Med Phys*. 2020;47(11):5779-5790.
26. Tiwari A. Monte Carlo simulations and phantom measurements towards more quantitative dosimetry and imaging in nuclear medicine. Ph.D. Thesis. University of Iowa; 2022.
27. Tiwari A, Graves S, Sunderland J. Measurements of dose point kernels using GATE Monte Carlo toolkit for personalized convolution dosimetry. *J Nucl Med*. 2019;60(1):274.

28. Tiwari A, Graves SA, Sunderland J. The impact of tissue type and density on dose point kernels for patient-specific voxel-wise dosimetry: a Monte Carlo investigation. *Radiat Res*. 2020;193(6):531-542.
29. Tiwari A, Merrick M, Graves SA, Sunderland J. Monte Carlo evaluation of hypothetical long axial field-of-view PET scanner using GE Discovery MI PET front-end architecture. *Med Phys*. 2022;49(2):1139-1152.
30. Tylski P, Pina-Jomir G, Bournaud-Salinas C, Jalade P. Tissue dose estimation after extravasation of (177)Lu-DOTATATE. *EJNMMI Phys*. 2021;8(1):33.
31. https://www.nndc.bnl.gov/nudat3/mird/, National Nuclear Data Center, NuDat3 (Nuclear Structure and Decay Data), Accessed April 17, 2023.
32. https://geant4-userdoc.web.cern.ch/UsersGuides/PhysicsReferenceManual/html/electromagnetic/introduction/livermore.html Geant4 Physics Reference Manual. Accessed date: May 20, 2023.
33. Zhu H, McNamara AL, McMahon SJ, et al. Cellular response to proton irradiation: a simulation study with TOPAS-nBio. *Radiat Res*. 2020;194(1):9-21.
34. Ramos-Méndez J, Perl J, Schuemann J, McNamara A, Paganetti H, Faddegon B. Monte Carlo simulation of chemistry following radiolysis with TOPAS-nBio. *Phys Med Biol*. 2018;63(10):105014.
35. Hanai R, Yazu M, Hieda K. On the experimental distinction between ssbs and dsbs in circular DNA. *Int J Radiat Biol*. 1998;73(5):475-479.
36. Schipler A, Iliakis G. DNA double-strand-break complexity levels and their possible contributions to the probability for error-prone processing and repair pathway choice. *Nucleic Acids Res*. 2013;41(16):7589-7605.
37. Tiwari A, Andriotty MS, Agasthya GA, Osborne DR, Kapadia AJ, Absorbed Doses from Accidental Extravasation of Radiotracers in PET Imaging. Abstract presented at: 65th Annual Meeting & Exhibition 2023.
38. Tiwari A, Andriotty M, Agasthya G, Sunderland J, Osborne D, Kapadia A. Assessment of impact of activity extravasation of radiopharmaceuticals in PET imaging. *J Nucl Med*. 2024;65(2):242321.
39. Valentin J. Avoidance of radiation injuries from medical interventional procedures. *Ann ICRP*. 2000;30(2):7-67.
40. Jaschke W, Schmuth M, Trianni A, Bartal G. Radiation-induced skin injuries to patients: what the interventional radiologist needs to know. *Cardiovasc Intervent Radiol*. 2017;40(8):1131-1140.
41. Chatterjee N, Walker GC. Mechanisms of DNA damage, repair, and mutagenesis. *Environ Mol Mutagen*. 2017;58(5):235-263.
42. Huang R, Zhou P-K. DNA damage repair: historical perspectives, mechanistic pathways and clinical translation for targeted cancer therapy. *Signal Transduct Target Ther*. 2021;6(1):254.
43. Vilenchik MM, Knudson AG. Endogenous DNA double-strand breaks: production, fidelity of repair, and induction of cancer. *Proc Natl Acad Sci USA*. 2003;100(22):12871-12876.
44. Penninckx S, Pariset E, Cekanaviciute E, Costes SV. Quantification of radiation-induced DNA double strand break repair foci to evaluate and predict biological responses to ionizing radiation. *NAR Cancer*. 2021;3(4):zcab046.

How to cite this article: Tiwari A, Andriotty M, Agasthya G, Sunderland JJ, Osborne DR, Kapadia AJ. Dosimetric and biological impact of activity extravasation of radiopharmaceuticals in PET imaging. *Med Phys*. 2024;1-13. https://doi.org/10.1002/mp.17520